Clinical Biomechanics 80 (2020) 105169

Contents lists available at ScienceDirect

Clinical Biomechanics

journal homepage: www.elsevier.com/locate/clinbiomech

An electromyography-assisted biomechanical cervical spine model: Model development and validation

Mina Alizadeh[a], Alexander Aurand[a], Gregory G. Knapik[a], Jonathan S. Dufour[a], Ehud Mendel[b], Eric Bourekas[c], William S. Marras[a,*]

[a] Spine Research Institute, The Ohio State University, 520 Baker Systems, 1971 Neil Avenue, Columbus, OH 43210, USA
[b] Department of Neurological Surgery, The Ohio State University, Columbus, OH 43210, USA
[c] Department of Radiology, The Ohio State University, Columbus, OH 43210, USA

ARTICLE INFO

Keywords:
Computational model
Neck model
Multi-body dynamics
Curved muscle model
Occupational neck injury

ABSTRACT

Background: In spite of the prevalence of occupational neck disorders as a result of work force fluctuating from industry to sedentary office work, most cervical spine computational models are not capable of simulating occupational and daily living activities whereas majority of cervical spine models specialized to simulate crash and impact scenarios. Therefore, estimating spine tissue loads accurately to quantify the risk of neck disorders in occupational environments within those models is not possible due to the lack of muscle models, dynamic simulation and passive spine structures.

Methods: In this effort the structure, logic, and validation process of an electromyography-assisted cervical biomechanical model that is capable of estimating neck loading under three-dimensional complex motions is described. The developed model was designed to simulate complex dynamic motions similar to work place exposure. Curved muscle geometry, personalized muscle force parameters, and separate passive and (electromyography-driven) active muscle force components are implemented in this model.

Findings: Calibration algorithms were able to reverse-engineer personalized muscle properties to calculate active and passive muscle forces of each individual.

Interpretation: This electromyography-assisted cervical spine model with curved muscle model is capable to accurately predict spinal tissue loads during isometric and dynamic head and neck activities. Personalized active and passive muscle force algorithms will help to more robustly investigate person-specific muscle forces and spinal tissue loads.

1. Introduction

Annual prevalence rates for neck pain have grown to 27–48% and are expected to continue to rise as a function of growing sedentary lifestyles and reliance on portable electronics (Côté et al., 2008, 2009). Hence, it is important to better appreciate the biomechanical forces acting on the cervical spine (CS) in order to understand and prevent workplace-related neck injuries, decrease their economic burden and improve the quality of life for those suffering.

While cervical spine models intended to assess activities of daily living are rare, previous impact models can inform model development (Alizadeh et al., 2020). Early on, discrete static impact models of the CS were developed to evaluate neck tissue injuries (Belytschko et al., 1978; Huston et al., 1978; Orne and Liu, 1971; Prasad and King, 1974). However, none of these models represented CS muscles as distinct elements and muscle representation is critical for non-impact models.

The CS models that did include muscles, represented them as spring elements (Deng and Goldsmith, 1987; Merrill et al., 1984; Williams and Belytschko, 1983). Although these models provide a better physical representation for muscle force direction, they relied on only the passive component of muscle force. As a result, these models were likely to significantly underestimate spinal load during non-impact scenarios by ignoring the contribution of active (contractile) muscle force.

Hill-type contractile muscle models were later implemented into CS musculoskeletal models (De Jager, 1996; van der Horst et al., 1997; Vasavada et al., 1998). To account for activation and create contractile muscle forces, these models used sets of activation curves, which are not able to provide realistic system dynamics.

* Corresponding author at: Biodynamics Laboratory, Spine Research Institute, The Ohio State University, Department of Integrated Systems Engineering, 1971 Neil Avenue, 210 Baker Systems Engineering, Columbus, OH 43210, USA.
E-mail address: marras.1@osu.edu (W.S. Marras).

https://doi.org/10.1016/j.clinbiomech.2020.105169
Received 28 January 2020; Accepted 31 August 2020
0268-0033/

Several models were developed later which used optimization algorithms to estimate muscle activation (Moroney et al., 1988; Snijders et al., 1991). However such optimization methods have been criticized as they fail to predict co-contraction of antagonist muscles which are evident in complex multi-planar motions (Choi and Vanderby Jr, 1999; Netto et al., 2008). Choi, 2003 demonstrated that co-contractions are essential to provide stability in human CS. In addition, the muscle forces predicted by an optimization approach depend greatly on the chosen objective function and sets of constraints (Choi, 2003; Mortensen et al., 2018), and disagreements have been observed between optimized muscle force and muscle activity as recorded by EMG (Moroney et al., 1988).

A few EMG-driven CS models have been developed to account for agonist and antagonist muscle co-activation (Huber, 2013; Netto et al., 2008). However, most existing CS models do not take into account person-specific musculoskeletal geometry, muscle parameters such as force-length and force-velocity, and active/passive muscle gain. All these factors are necessary to represent specific pathologies in clinical applications (Klein Horsman et al., 2007) and to describe the morphology of specific populations (Cazzola et al., 2017).

In this study, we developed and validated a novel personalized EMG-assisted model that overcomes many of the previously discussed limitations in order to better predict spinal tissue loading during complex dynamic occupational tasks. Since this model will be used for understanding neck loading under daily living (non-impact) conditions, it was validated for isometric and dynamic conditions.

2. Methods

2.1. Model development

2.1.1. Model structure

In this effort, a well-developed and validated lumbar spine model structure was crated based upon our previous effort building a canine EMG-driven CS model (Alizadeh et al., 2017; Dufour et al., 2013a; Hwang et al., 2016).

A conceptual diagram for the EMG-assisted CS model (CSM) developed in this study is shown in Fig. 1, which illustrates the inner working of the model. Model inputs included: 1) Dynamic location and orientation of body segments, including head and neck, determined from an optical motion capture system; 2) Musculoskeletal geometry including precise centroid lines of action (LOA) for 11 bilateral pairs of muscles, derived from MRI; 3) Surface electromyography signals recorded at 6 bilateral locations of accessible major force-producing neck muscles; and 4) Three-dimensional external forces and moments, as measured by force transducers.

Model simulations were performed in Adams (MSC Software Corporation, Santa Ana, CA, USA), a multi-body dynamic motion simulation solution for analyzing the complex behavior of mechanical assemblies.

2.1.2. EMG-assisted CSM musculoskeletal geometry

The proportions and shape of the head and neck geometry were obtained from the MRI of an individual subject. The inertial properties of the cervical vertebrae were obtained from literature (van Lopik and Acar, 2007).

Individual CS muscles were traced and labeled in MR transverse slices. The centroid of each muscle was then identified on each slice (Alizadeh et al., 2018). Muscle LOAs were developed for 11 pairs of CS muscles including upper trapezius, semispinalis capitis, semispinalis cervicis, splenius capitis, splenius cervicis, levator scapula, sternocleidomastoid, hyoid muscle group, longus capitis, longus colli, and intertransversari (Fig. 2). Intersegmental points attached to the vertebral bodies, commonly referred to as via-points, were used in order to let the muscle LOA follow CS curvature during complex dynamic neck activities (Table 1).

2.1.3. EMG-assisted CSM personalized muscle force algorithm

The force of each individual muscle was obtained from a Hill-type physiological muscle model. This model includes active (contractile) and passive muscle force components (Eq. (1)).

$$F_i(t) = ActiveF_i(t) + PassiveF_i(t)$$
$$F_i(t) = (GainRatio_i \times CSA_i \times EMG(t)_i \times F_{l,active}[L_i(t)] \times F_v[v_i(t)]) + (Gain_i \times CSA_i \times F_{l,passive}[L_i(t)]) \quad (1)$$

According to (Dufour et al., 2013a), gain ratio (GR) was used for active mucle force calculation in order to extend the model usability to both healthy and injured subjects, since subjects with spine disorders are not able to perform maximum voluntary contraction (MVCs). Due to the complex muscular structure of CS and limitations associated with sEMG, 6 bilateral pairs of EMG signals were used to model the activation of 11 modeled muscle pairs. The muscle EMG signals "driving" the various muscles can be seen in Table 2 (Alizadeh et al., 2018). The surrogate sEMG for inaccessible muscles were chosen based on the similarity of muscle function and attachments. The semispinalis cervicis, splenius capitis, longus capitis, longus colli, and intertransversari were surrogated with semispinalis capitis, splenius capitis, hyoid, hyoid and levator scapula sEMG signals, respectively.

Eq. 2 shows the elements of the F-L modulation (Horst and Der, 2002). Based on this equation, the muscle is capable of producing optimal force when positioned at its optimal length(l_0).

$$f_{l,active}[L_i(t)] = k_1\left(\frac{l - l_0}{l_0}\right)^2 + 1 \quad (2)$$

Muscle force-velocity modulations (Eqs. (3) and (4)) account for the muscle's capability to generate force during concentric and eccentric exertions as a function of muscle normalized velocity (Cadova et al., 2014).

$$f[v_i(t)]_{Concentic} = \frac{10 - v_{normalized}}{10 + {v_{normalized}}/{k_2}} \quad (3)$$

$$f[v_i(t)]_{Eccentric} = 1.8 - \frac{0.8\left(1 + {v_{normalized}}/{10}\right)}{1 - 0.765.\ {v_{normalized}}/{k_{3.10}}} \quad (4)$$

The passive component of muscle force was derived from the product of: (1) gain, (2) cross-sectional area and (3) the force-length modulation. Muscle gain represents the maximum force per unit area of the muscle. Eq. (5) shows the passive force-length relationship and its components (Woittiez et al., 1983, 1984, 1985).

$$f_{l,passive}[L_i(t)] = e^{k_4\left(\frac{l}{l_0}\right)} \quad (5)$$

An optimization algorithm selects personalized physiological muscle parameters to minimize dynamic root mean square error (RMSE) between person-specific measured "external" moments and model-predicted "internal" moments at seven CS levels in the sagittal, lateral and axial planes.

In this model, muscle force varies along the length of the cervical spine based on the number of muscle attachments. It is assumed that the muscle picks up a fraction of its total force at each origin, inversely proportional to the number of origins, and likewise drops a fraction at each insertion (Table 1). Each muscle segment is a muscle component between consecutive via-points.

2.1.4. EMG-assisted CSM ligament model

The ligaments were modeled as single force vectors located between ligament attachments, determined from anatomy books (Boyd et al., 2001; Lang, 1993). Ligament properties were modeled as nonlinear tension-only spring elements with material properties obtained from Mattucci et al., 2013; Mattucci and Cronin, 2015. The ligament force expression is shown in Eqs. (6) and (7) (Mattucci and Cronin, 2015).

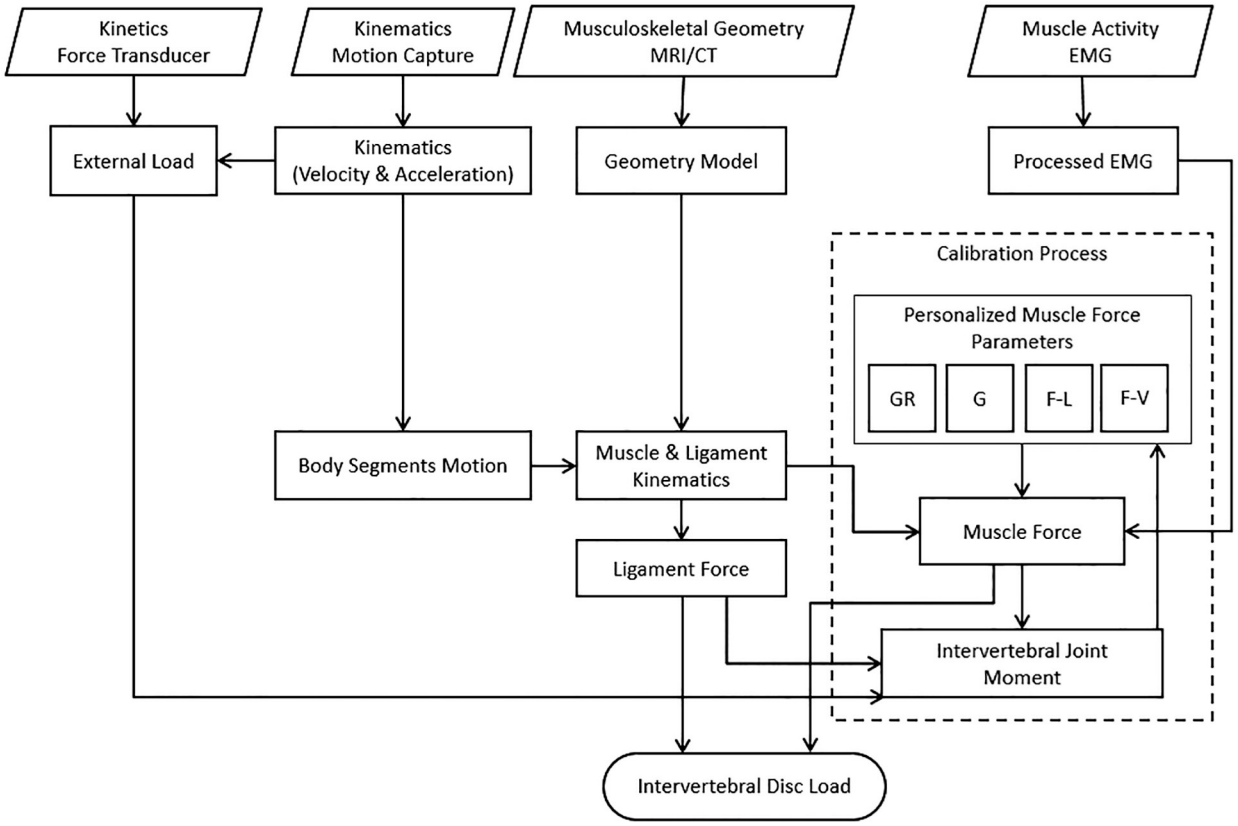

Fig. 1. EMG-assisted cervical spine model conceptual diagram. Dashed line box encompasses calibration process in which personalized muscle force parameters such ass gain-ratio (GR), passive gain (G), active and passive force-length (F–L) and force-velocity (F–V) modulation are optimized.

$$\text{Toe: } F = C_1(\exp(C_2.\ dl) - 1) dl^{m*} \text{ for } dl < dl^* \quad (6)$$

$$\textit{Linear: } F = F_{dl^*} + (dl - dl^*)C_3 \text{ for } dl > dl^* \quad (7)$$

Ligamentum flavum (LF), anterior longitudinal (ALL), posterior longitudinal (PLL), interspinous (ISL), transverse ligament (TL), tectorial membrane (TM), apical ligament (AL), posterior atlanto-occipital ligament (PAOL), posterior atlanto-axial ligament (PAAL), anterior atlanto-occipital ligament (AAOL), anterior atlanto-axial ligament (AAAL) were represented in this model.

2.1.5. EMG-assisted CSM intervertebral disc and facet model

The translational stiffness of intervertebral discs was simulated by linear viscoelastic "bushing elements" in MSC Adams. A 'bushing' constraint allows all translational and rotational degrees of freedom to be restricted by spring and damper relationships. Translational stiffness and translational and rotational damping properties for bushing elements were obtained from (van Lopik and Acar, 2007).The rotational stiffness of intervertebral discs was modeled by nonlinear restoring moment dependent on the joint's multi-planar rotation (Panjabi et al., 2001). It is not sufficient because it is not valid to translate EMG signals directly to muscle force. Contact in the facet joint is modeled by linear translational springs (Horst and Der, 2002).

2.2. Model validation

2.2.1. Participants

The ten subjects (5 male, 5 female) who participated in this study were free from any musculoskeletal neck discomfort or abnormality at the time, and did not have any prior neck disorder, injury or surgery. Mean values and standard deviations of age, body mass, and stature of the subjects were 25.3 (4.3) years, 69.8 (7.3) kg, and 170.5 (10.2) cm, respectively.

2.2.2. Instrumentation

Muscle activities were collected via sEMG (Motion Lab Systems MA300-XVI, Baton Rouge, Louisiana, USA) over fourteen CS muscles. Customized Laboratory software and a data acquisition system (NI USB-6225, National Instruments, Austin, TX, USA) were used to collect all signals simultaneously and run the biomechanical model. Subjects exerted against a small custom-built six-axis load cell (HT0825, Bertec, Worthington, OH, USA) mounted on a custom height adjustable frame. Kinematic data of individual body segments were collected via a 42-camera optical motion capture system (Optitrack Prime 41, NaturalPoint, Corvallis, OR, USA) with a 120 Hz sampling rate.

Electromyography activity of the muscles was collected with surface electrodes and sampled at 1000 Hz. Signals were notch filtered at 60 Hz and its aliases (up to 480 Hz), band-pass filtered at 30–450 Hz, and then were rectified and smoothed using a fourth order low pass filter with a cutoff frequency of 1.59 Hz. Kinetic data were captured at 1000 Hz.

2.2.3. Testing procedure

After arriving at the laboratory, subjects gave informed consent per the University IRB.

Surface electrodes were placed over fourteen CS muscles based on standard placement guidelines (Alizadeh et al., 2018), Fig. 3. Motion capture markers were placed over 41 different locations on the body as set by standard placement locations from OptiTrack's motion capture software.

The *isometric* trials required subjects to stand in a neutral posture while wearing an augmented helmet connected to the load cell and custom-built frame (Fig. 4). The height of the frame was adjusted to subject's height in standing posture. Tasks included isometric neck flexion, extension, right/left lateral bending, and right/left axial rotation. The participants were instructed to exert force ramping up to their maximum comfortable exertion. The *dynamic* tasks involved single-

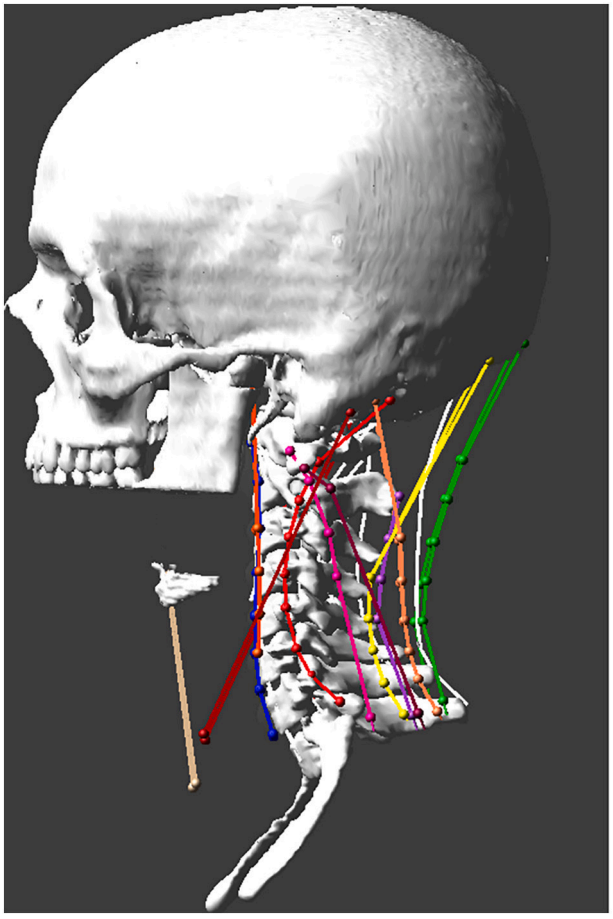

Fig. 2. Three-dimensional graphical representation of musculoskeletal structure of CS Model. Note: colored lines illustrate CS model muscles curved LOA while each color belongs to a particular muscle. Multiple points along the muscle LOA indicates the "via-points".

plane motions such as neck flexion, extension, lateral bending, and axial rotation, performed in a randomized order. Each task was performed twice. To limit the effects of fatigue, subjects were allowed to rest between exertions.

2.2.4. Data analysis

The validation procedure of the model was based on a comparison of intervertebral joint moments between externally measured moments (based on kinematics and kinetics) and model-predicted moments (based on muscles, ligaments and discs) in the sagittal and lateral planes from C7/T1 to C0/C1 levels. Multi-planar (sagittal and lateral planes) weighted squared correlation coefficient (R^2), average absolute error (AAE), and peak-normalized average absolute error (PNAAE) measurements were used to evaluate the model performance.

3. Results

3.1. Isometric tasks

Fig. 5(a), shows the mean and standard deviations of multi-planar average R^2 for isometric flexion, extension and lateral neck bending tasks. During the isometric tasks, the mean multi-planar average R^2 varied from 0.70–0.86. This indicates that the moments predicted by the model follow the pattern of the measured external moment very well for isometric tasks.

Table 3 shows a summary of the mean and standard deviation of multi-planar average absolute error (AAE) for all disc levels in isometric

Table 1
Cervical spine model muscle components.

Muscle name	T1	C7	C6	C5	C4	C3	C2	C1	C0	Segment 1	Segment 2	Segment 3	Segment 4	Segment 5	Segment 6	Segment 7	Segment 8
Right sternocleidomastoid	Yes	No	No	No	No	No	No	No	Yes	1	None	None	None	None	None	None	None
Left sternocleidomastoid	Yes	No	No	No	No	No	No	No	Yes	1	None	None	None	None	None	None	None
Right levator scapula	Yes	No	No	No	Yes	Yes	Yes	Yes	No	1	0.75	0.5	0.25	None	None	None	None
Left levator scapula	Yes	No	No	No	Yes	Yes	Yes	Yes	No	1	0.75	0.5	0.25	None	None	None	None
Right trapezius	Yes	No	No	Yes	Yes	Yes	Yes	Yes	Yes	1	1	1	1	1	1	None	None
Left trapezius	Yes	No	No	Yes	Yes	Yes	Yes	Yes	Yes	1	1	1	1	1	1	None	None
Right splenius capitis	Yes	Yes	Yes	Yes	Yes	Yes	No	No	Yes	0.375	0.5	0.625	0.75	0.875	1	None	None
Left splenius capitis	Yes	Yes	Yes	Yes	Yes	Yes	No	No	Yes	0.375	0.5	0.625	0.75	0.875	1	None	None
Right splenius cervicis	Yes	No	No	No	No	No	Yes	Yes	No	1	0.5	None	None	None	None	None	None
Left splenius cervicis	Yes	No	No	No	No	No	Yes	Yes	No	1	0.5	None	None	None	None	None	None
Right semispinalis capitis	Yes	Yes	Yes	Yes	Yes	No	No	No	Yes	0.6	0.7	0.8	0.9	1	None	None	None
Left semispinalis capitis	Yes	Yes	Yes	Yes	Yes	No	No	No	Yes	0.6	0.7	0.8	0.9	1	None	None	None
Left semispinalis cervicis	Yes	No	No	Yes	Yes	Yes	Yes	No	No	1	0.75	0.5	0.25	None	None	None	None
Right semispinalis cervicis	Yes	No	No	Yes	Yes	Yes	Yes	No	No	1	0.75	0.5	0.25	None	None	None	None
Right hyoid	Yes	No	No	No	No	No	No	No	Yes	1	None	None	None	None	None	None	None
Left hyoid	Yes	No	No	No	No	No	No	No	Yes	1	None	None	None	None	None	None	None
Right longus capitis	No	No	Yes	Yes	Yes	Yes	No	No	Yes	0.25	0.5	0.75	1	None	None	None	None
Left longus capitis	No	No	Yes	Yes	Yes	Yes	No	No	Yes	0.25	0.5	0.75	1	None	None	None	None
Right longus colli	Yes	Yes	Yes	Yes	Yes	Yes	Yes	Yes	No	0.5	0.46	0.58	0.71	0.83	0.83	0.83	None
Left longus colli	Yes	Yes	Yes	Yes	Yes	Yes	Yes	Yes	No	0.5	0.46	0.58	0.71	0.83	0.83	0.83	None
Right intertransversari	Yes	Yes	Yes	Yes	Yes	Yes	Yes	Yes	Yes	1	1	1	1	1	1	1	1
Left intertransversari	Yes	Yes	Yes	Yes	Yes	Yes	Yes	Yes	Yes	1	1	1	1	1	1	1	1

Table 2
Recorder EMG and its paired muscle.

Nominal sEMG muscle group	Modeled muscle(s)
Semispinalis capitis	Semispinalis capitis
	Semispinalis cervicis
Splenius capitis	Splenius capitis
	Splenius cervicis
Hyoid	Hyoid
	Longus capitis
	Longus colli
Levator scapula	Levator scapula
	Intertransversari

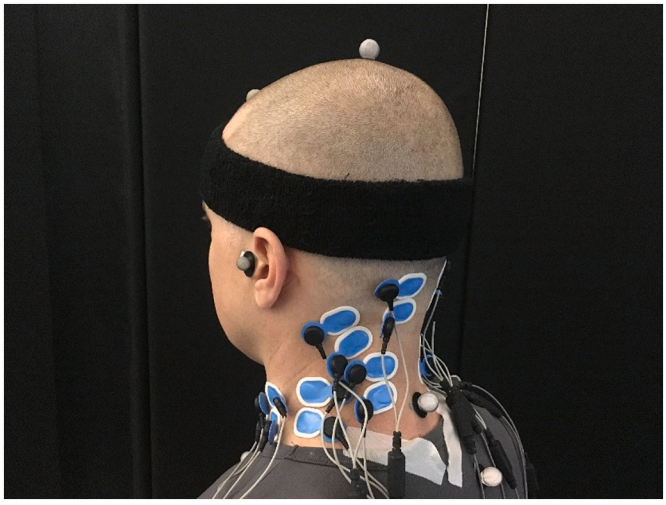

Fig. 3. Surface EMG locations for cervical spine muscles.

flexion, extension and lateral bending tasks. During the isometric tasks, weighted AAEs ranged from 1.17–3.32 Nm. Fig. 5(b), shows mean and standard deviations of multi-planar peak normalized average absolute error (PNAAE) for the isometric flexion, extension and lateral bending tasks.

3.2. Dynamic tasks

Fig. 6(a), shows mean and standard deviations of multi-planar average R^2 for the dynamic flexion, extension and lateral bending tasks. In terms of model performance during dynamic tasks, the means and standard deviations of the multi-planar average R^2s at each disc level from C7/T1 to C0/C1 were 0.89 (0.02), 0.88 (0.01), 0.88(0.02), 0.88 (0.02), 0.89 (0.01), 0.86 (0.02), 0.75 (0.06), and 0.74 (0.07), respectively. This indicates that the model-predicted moments follow the pattern of the measured external moment very well for dynamic tasks. Note that there is a slight decrement in performance at the more superior levels of the CS.

Table 3 shows the summary of the means and standard deviations for the multi-planar average absolute error (AAE) for all disc levels in dynamic flexion, extension and lateral bending. Among the dynamic tasks, weighted AAE from C7/T1 to C0C1 were 1.76 (0.11) Nm, 1.05 (0.18) Nm, 0.91 (0.23) Nm, 0.78 (0.18) Nm, 0.75 (0.12) Nm, 0.91 (0.36) Nm, 1.25 (0.73) Nm, and 1.64 (0.67) Nm, respectively. Fig. 6(b), shows the means and standard deviations of the multi-planar peak normalized average absolute error (PNAAE) for dynamic flexion, extension and lateral bending tasks.

4. Discussion

4.1. Model structure

The present paper describes the model structure and validation of a newly-developed EMG-assisted CS model. Fig. 2 shows a three-dimensional representation of the CS musculoskeletal geometry. The present model overcomes many of the limitations of existing CS models (ref to literature review article) by introducing important new features. The advantage of this model is that it brings together a variety of novel and existing features in order to improve accuracy and increase its ability to assess injury risk in occupational settings.

First, the model structure is multi-dimensional and is capable of considering the dynamic response of individuals. The CS moments and tissue loads are derived from dynamic muscle force vectors and internal neck muscle moment arms.

Second, the model implements MRI-derived curved muscle geometry with via-points. Realistic representation of muscle LOA in biomechanical models are important for determining muscle moment generating potential (Vasavada et al., 2008). Due to the limitations of sEMG in distinguishing between individual fascicle activities, we represented each muscle with a single curved LOA. When assuming one LOA for a muscle with several fascicles, the centroid path was determined to be the best representation for the LOA (An et al., 1981) as showed sufficiently small deviation from the standard muscle centroid path obtained from MRI in multiple neck postures (Suderman et al., 2012; Suderman and Vasavada, 2017).

Third, a Hill muscle model was fully implemented in this model. In this study, we employed a muscle force calculation algorithm in which both active and passive Hill muscle elements are taken into account. A muscle's length and contraction velocity have a profound effect on its ability to produce force and are accounted for in this model via force-length and force-velocity modulation factors. The developed model specifically determines these modulations from the subject's kinematics and considers their effect on muscle force magnitude.

Fourth, realistic consideration for muscle co-contraction was adopted by incorporating sEMG signals as indicators of muscle activation. The majority of previously-developed cervical spine models attempted to predict muscle responses to a motion using simplifying assumptions or optimization algorithms. Those approaches generally fail to predict co-contraction of antagonist muscles (Choi and Vanderby Jr, 1999; Netto et al., 2008), which are seen in complex dynamic motions. Studies have shown that ignoring co-activation could result in underestimating spinal load by 45%–70% (Granta and Marras, 1999). Choi, 2003 showed that CS stability relies on agonist and antagonist co-contractions. Therefore, it is not surprising that through these non-physiologic techniques, no study to date has been able to model the head in equilibrium at upright posture under the effect of gravity (Chancey et al., 2003). On the other hand, the EMG-based modeling approach adopted in this model is able to account for individual differences in activation pattern and magnitude.

Finally, the developed EMG-assisted CS model is unique in that it is personalized in many ways: (1) The musculoskeletal structure is scaled and positioned for each subject based on the segment dimensions; (2) Model kinematics are multi-dimensional and capable of considering the dynamic response of the individual. This allows the muscle LOAs to be oriented according to the subject's dynamic posture; (3) Individual muscle recruitment patterns were considered through sEMG; (4) Muscle properties were optimized for each subject.

4.2. Model validation

During the validation study, we intended to evaluate the ability of the model to predict spine loads that are biomechanically accurate and physiologically plausible. This was accomplished by examining the model predictions of internal moments over time and comparing this

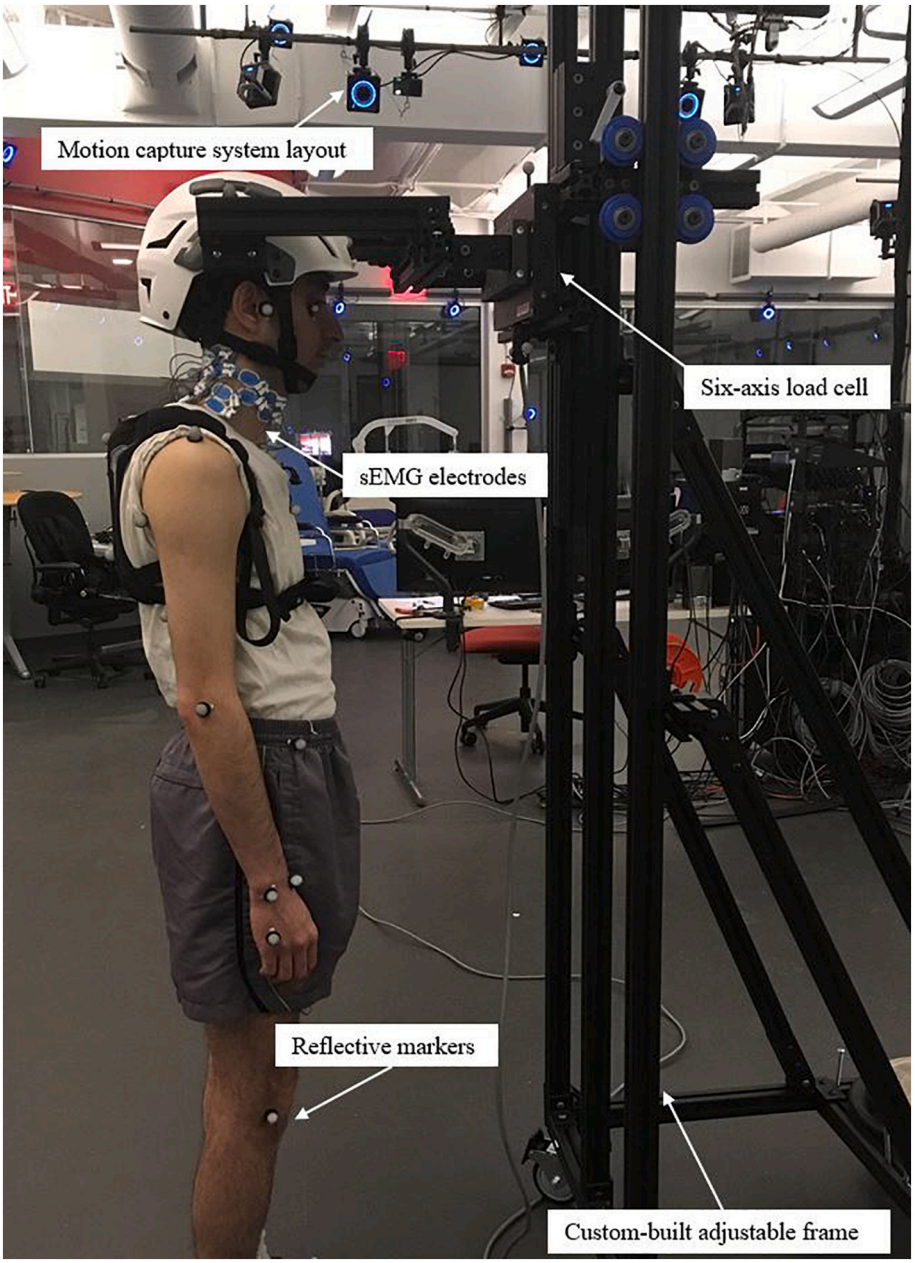

Fig. 4. Photo showing experimental setup for isometric contractions.

time history to the measured external moments. Overall, the amount of error between our model estimations and the externally measured moments were generally less than 25%. These findings suggest that our model, while not perfect, is behaving reasonably well. The model performed extremely well over dynamic motions and could account for at least 80% of the variability in multi-planar spinal moments from level to level and could generally predict spinal moments with less than 25% average error from level to level. Thus, under both static and dynamic conditions, the model performed well.

In the current study, multi-planar weighted fidelity measures rather than single-planar measures were used as a performance indicator. Summation of single-planar measures (sagittal and lateral planes) were weighted relative to peak in-plane external moments, giving more significance to the planes of the body that experience more significant loads. Since the axial plane motion in isometric trials couldn't be isolated, the axial plane was excluded from the calculations. The functional validity of this measure was reported in a previous study (Dufour et al., 2013b).

The results indicated that moment-matching performance was better for flexion in dynamic tasks, while it is better for extension in isometric tasks. This may be the result of poor representation of the neural drive of extensor muscles. Semispinalis capitis and splenius capitis channels drove the semispinalis cervicis and splenius cervicis, respectively. The upper trapezius signal was not used to drive all the extensors since studies had shown that the splenius capitis activation pattern is subject specific and significantly different from other cervical spine extensors (Siegmund et al., 2007). At lower levels of activation, during dynamic tasks, signals from the semispinalis capitis and splenius capitis muscles may not have been strong enough to be picked up by sEMG accurately or were masked by cross-talk with their neighbor superficial muscles such as trapezius. Therefore, the extensor muscle contribution to balancing the external moments were underestimated. On the other hand, during isometric exertions, higher level of activation produced stronger signals from extensor muscles that result in better extensor muscle contribution prediction. Studies utilizing needle electrodes for the cervical spine deep muscles may be useful in testing this

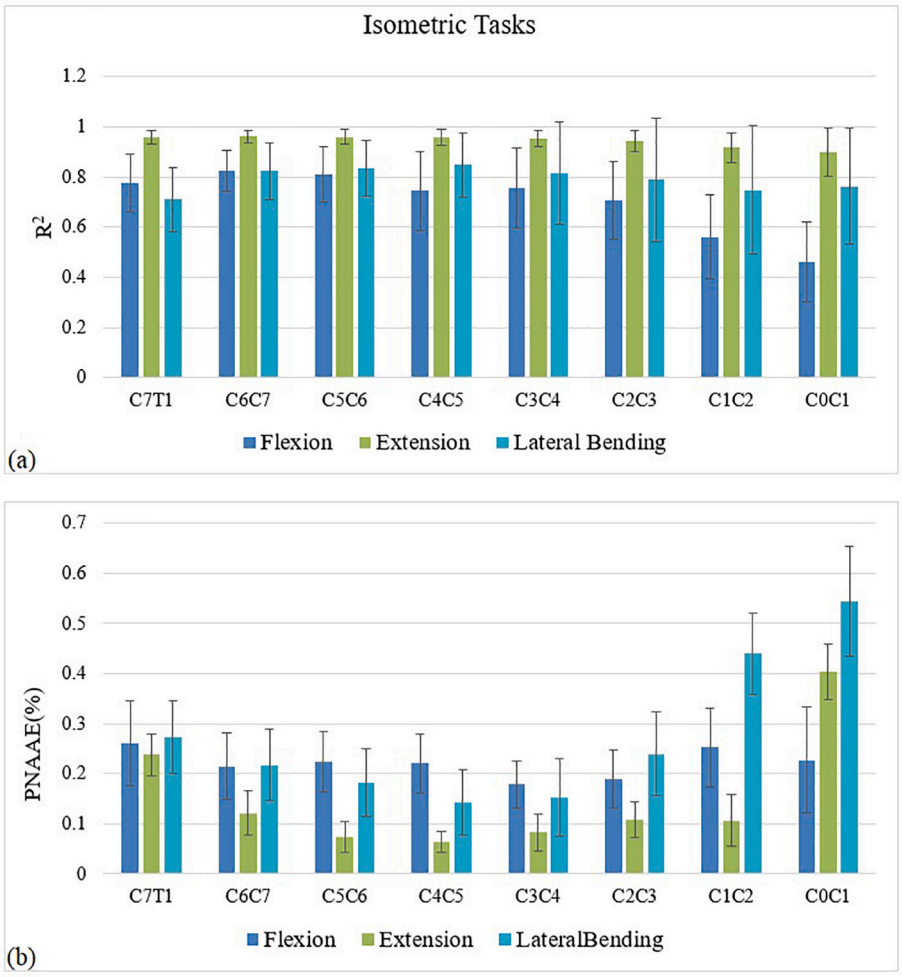

Fig. 5. (a) Mean and standard deviation of multi-planar R^2 at various levels of the CS during isometric flexion, extension and lateral bending tasks. (b) Mean and standard deviation of multi-planar peak normalized average absolute error (PNAAE) at various levels of the CS during isometric flexion, extension and lateral bending tasks.

Table 3
Mean (standard deviation) of multi-planar AAE at cervical spine levels for isometric and dynamic tasks.

	AAE (Nm)			AAE (Nm)		
	Isometric tasks			Dynamic tasks		
	Flexion	Extension	Lateral bending	Flexion	Extension	Lateral bending
C7/T1	2.54 (2.22)	5.07 (2.72)	2.33 (1.73)	1.65 (0.26)	1.92 (0.95)	1.71 (1.35)
C6/C7	2.24 (2.17)	2.37 (1.67)	1.92 (1.29)	0.79 (0.23)	1.23 (0.37)	1.13 (1.12)
C5/C6	2.20 (2.07)	1.34 (1.04)	1.58 (1.32)	0.60 (0.14)	1.17 (0.34)	0.96 (1.56)
C4/C5	2.11 (2.17)	1.02 (0.70)	1.09 (0.90)	0.54 (0.11)	0.99 (0.35)	0.80 (1.7)
C3/C4	1.74 (2.15)	1.12 (0.79)	0.89 (0.61)	0.60 (0.06)	0.74 (0.32)	0.90 (1.41)
C2/C3	1.55 (1.89)	1.23 (1.04)	1.12 (0.97)	0.70 (0.07)	0.61 (0.49)	1.43 (1.53)
C1/C2	1.13 (0.88)	0.824424 (0.60)	1.55 (1.81)	0.73 (0.1)	0.73 (0.31)	2.30 (2.26)
C0/C1	0.90 (0.73)	0.67 (0.39)	2.82 (4.99)	0.88 (0.15)	1.54 (0.9)	2.51 (2.26)

hypothesis.

In general, model performance for both isometric and dynamic tasks were comparable. Model performance was greater in the middle cervical spine levels (C5/C6-C2/C3) and lower at the upper levels (C0/C1 and C1/C2). Some of the possible explanations for lower performance in the upper cervical spine could be: 1) there are several deep muscles such as rectus capitis major & minor, along with the oblique capitis superior and inferior, which have not been modeled in this study due to the lack of information on their neural activity. These muscles have large cross-sectional areas and are believed to contribute in head movement and posture maintenance. Therefore, their active and passive contribution to the model moment production was limited; 2) Craniovertebral joints are the most complex joints in the spinal column, not only anatomically but with multiple sources of passive force producers. The vertebral bodys' complex geometry, along with several ligaments and facet and synovial joints that are all unique to this region (allowing greater range of motion), are extremely difficult to properly model. Considering the limitations of the current model in representing the craniovertebral passive force elements, one would expect to observe the greatest model error for these joints.

Currently there are very limited criteria with which to compare the model's spinal loads against, aside from failure loads of functional spinal units. As mentioned previously, most of the cervical spine models available in the literature were developed for crash testing. Low magnitude loads and muscular activation during dynamic tasks were rarely evaluated. This lack of experimental criteria makes validation of this

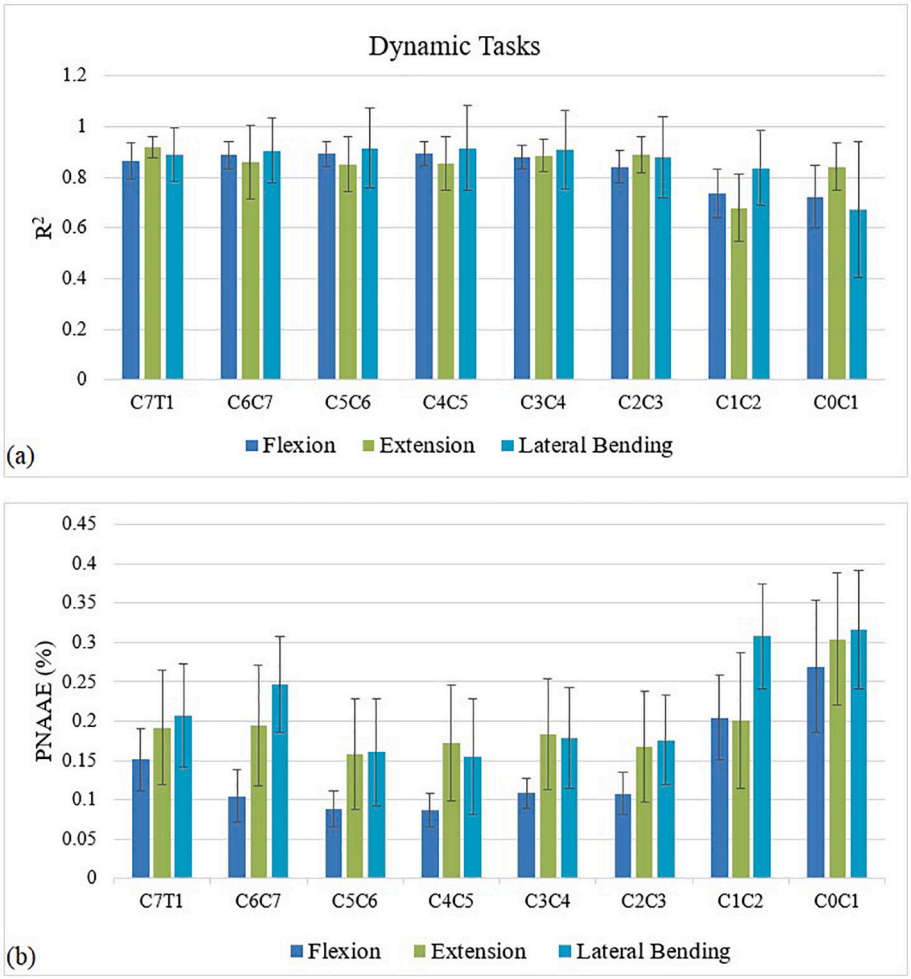

Fig. 6. (a) Means and standard deviations of multi-planar R^2 at various levels of CS during dynamic flexion, extension and lateral bending tasks. (b) Means and standard deviations of multi-planar peak normalized average absolute error (PNAAE) at various levels of CS during dynamic flexion, extension and lateral bending tasks.

model by comparing to the reported data very difficult. Therefore, in this study the validation process was based primarily on the model's capability to estimate internal moments that match the measured external moments.

4.3. Model limitation

Several limitations should be acknowledged. First, our model was only tested in neck bending and twisting conditions. Validation of other types of occupational tasks would need to be tested. Second, there are several muscles in the cervical spine inserting into the scapula, sternum, and clavicle, which result in a coupling of the neck and the shoulder moments. Accurate estimation of the motion and orientation of these joints would lead to more accurate lines of action near the base of the cervical spine. Third, facet joints or uncovertebral joints were not given full attention. Proper contact force implementation would improve model performance in dynamic tasks. Fourth, while the ligament representation in the model is believed to be reasonable in the middle and lower levels (Mattucci et al., 2013), it should be improved in the upper cervical spine. Fifth, the nuchal ligament has not been modeled in this study due to its complex structure and limited knowledge of its biomechanical properties. Finally, several deep cervical spine muscles have not been modeled due to the lack of neural activation information. A hybrid-EMG model, in which the contribution of deep muscles to spinal moments could be estimated through an EMG-based optimization algorithm could greatly improve the performance of the current model.

5. Conclusion

In this article, the model structure and validation process of a novel EMG-assisted cervical spine model was described. This model introduced several new features including precise curved muscle geometry, accurate representation of active and passive muscle force, personalized muscle force-length and force-velocity relationships, and realistic EMG-based muscle force calculation. This model allows for the assessment of person-specific spine tissue loading along the entire cervical spine during complex dynamic exertions. This model has been examined to validate its performance during isometric static and dynamic exertions. This model was able to reliably evaluate three-dimensional spinal loads as a function of various external loads and neck motions. Collectively, the results suggest that the predicted muscle forces and spinal loads from this model would be acceptable for assessments in multi-planar activities of daily living.

Declaration of Competing Interest

None.

References

Alizadeh, M., Knapik, G.G., Dufour, J.S., Zindl, C., Allen, M.J., Bertran, J., Fitzpatrick, N., Marras, W.S., 2017. An EMG-driven biomechanical model of the canine cervical spine. J. Electromyogr. Kinesiol. Off. J. Int. Soc. Electrophysiol. Kinesiol. 32, 101–109.

Alizadeh, M., Knapik, G.G., Marras, W.S., 2018. Application of MR-derived cross-sectional guideline of cervical spine muscles to validate neck surface electromyography placement. J. Electromyogr. Kinesiol. 43, 127–139.

Alizadeh, M., Knapik, G.G., Mageswaran, P., Mendel, E., Bourekas, E., Marras, W.S., 2020. Biomechanical musculoskeletal models of the cervical spine: a systematic literature review. Clin. Biomech. 71, 115–124.

An, K.N., Hui, F.C., Morrey, B.F., Linscheid, R.L., Chao, E.Y., 1981. Muscles across the elbow joint: a biomechanical analysis. J. Biomech. 14, 659–669.

Belytschko, T., Schwer, L., Privitzer, E., 1978. Theory and application of a three-dimensional model of the human spine. Aviat. Space Environ. Med. 49, 158–165.

Boyd, J.S., Paterson, C., May, A.H., 2001. Clinical Anatomy of the Dog & Cat. Harcourt Publishers Limited, Jamestown Road, London.

Cadova, M., Vilimek, M., Daniel, M., 2014. A comparative study of muscle force estimates using Huxley's and Hill's muscle model. Comput. Methods Biomech. Biomed. Eng. 17, 311–317.

Cazzola, D., Holsgrove, T.P., Preatoni, E., Gill, H.S., Trewartha, G., 2017. Cervical spine injuries: a whole-body musculoskeletal model for the analysis of spinal loading. PLoS One 12.

Chancey, V.C., Nightingale, R.W., Van Ee, C.A., Knaub, K.E., Myers, B.S., 2003. Improved estimation of human neck tensile tolerance: reducing the range of reported tolerance using anthropometrically correct muscles and optimized physiologic initial conditions. Stapp Car Crash J. 47, 135–153.

Choi, H., 2003. Quantitative assessment of co-contraction in cervical musculature. Med. Eng. Phys. 25, 133–140.

Choi, H., Vanderby Jr., R., 1999. Comparison of biomechanical human neck models: muscle forces and spinal loads at C4/5 level. J. Appl. Biomech. 15, 120–138.

Côté, P., van der Velde, G., Cassidy, J.D., Carroll, L.J., Hogg-Johnson, S., Holm, L.W., Carragee, E.J., Haldeman, S., Nordin, M., Hurwitz, E.L., Guzman, J., Peloso, P.M., 2008. Bone and joint decade 2000–2010 task force on neck pain and its associated disorders, The burden and determinants of neck pain in workers: results of the bone and joint decade 2000–2010 task force on neck pain and its associated disorders. Spine 33, S60–S74.

Côté, P., Kristman, V., Vidmar, M., Van Eerd, D., Hogg-Johnson, S., Beaton, D., Smith, P.M., 2009. The prevalence and incidence of work absenteeism involving neck pain: a cohort of Ontario lost-time claimants. J. Manip. Physiol. Ther. Neck Pain Task Force Spec. Suppl. 32, S219–S226.

De Jager, M., 1996. Mathematical Head-Neck Models for Acceleration Impacts.

Deng, Y.-C., Goldsmith, W., 1987. Response of a human head/neck/upper-torso replica to dynamic loading—II. Analytical/numerical model. J. Biomech. 20, 487–497.

Dufour, J.S., Marras, W.S., Knapik, G.G., 2013a. An EMG-assisted model calibration technique that does not require MVCs. J. Electromyogr. Kinesiol. Off. J. Int. Soc. Electrophysiol. Kinesiol. 23, 608–613.

Dufour, J.S., Marras, W.S., Knapik, G.G., 2013b. An EMG-assisted model calibration technique that does not require MVCs. J. Electromyogr. Kinesiol. 23, 608–613.

Granta, K.P., Marras, W.S., 1999. Relation between spinal load factors and the high-risk probability of occupational low-back disorder. Ergonomics 42, 1187–1199.

Horst, M.J., Der, V., 2002. Human Head Neck Response in Frontal, Lateral and Rear End Impact Loading: Modelling and Validation.

Huber, Z.E., 2013. Creation and Validation of a Dynamic, EMG-Driven Cervical Spine Model. The Ohio State University.

Huston, R.L., Huston, J.C., Harlow, M.W., 1978. Comprehensive, three-dimensional head-neck model for impact and high-acceleration studies. Aviat. Space Environ. Med. 49, 205–210.

Hwang, J., Knapik, G.G., Dufour, J.S., Aurand, A., Best, T.M., Khan, S.N., Mendel, E., Marras, W.S., 2016. A biologically-assisted curved muscle model of the lumbar spine: model structure. Clin. Biomech. 37, 53–59.

Klein Horsman, M.D., Koopman, H.F.J.M., van der Helm, F.C.T., Prosé, L.P., Veeger, H.E.J., 2007. Morphological muscle and joint parameters for musculoskeletal modelling of the lower extremity. Clin. Biomech. 22, 239–247.

Lang, J., 1993. In: Verlag, G. Thieme (Ed.), Clinical Anatomy of the Cervical Spine. Thieme Medical Publishers, Stuttgart; New York; New York.

Mattucci, S.F.E., Cronin, D.S., 2015. A method to characterize average cervical spine ligament response based on raw data sets for implementation into injury biomechanics models. J. Mech. Behav. Biomed. Mater. 41, 251–260.

Mattucci, S.F.E., Moulton, J.A., Chandrashekar, N., Cronin, D.S., 2013. Strain rate dependent properties of human craniovertebral ligaments. J. Mech. Behav. Biomed. Mater. 23, 71–79.

Merrill, T., Goldsmith, W., Deng, Y.C., 1984. Three-dimensional response of a lumped parameter head-neck model due to impact and impulsive loading. J. Biomech. 17, 81–95.

Moroney, S.P., Schultz, A.B., Miller, J.A., 1988. Analysis and measurement of neck loads. J. Orthop. Res. Off. Publ. Orthop. Res. Soc. 6, 713–720.

Mortensen, J.D., Vasavada, A.N., Merryweather, A.S., 2018. The inclusion of hyoid muscles improve moment generating capacity and dynamic simulations in musculoskeletal models of the head and neck. PLoS One 13, e0199912.

Netto, K.J., Burnett, A.F., Green, J.P., Rodrigues, J.P., 2008. Validation of an EMG-driven, graphically based isometric musculoskeletal model of the cervical spine. J. Biomech. Eng. 130, 031014.

Orne, D., Liu, Y.K., 1971. A mathematical model of spinal response to impact. J. Biomech. 4, 49–71.

Panjabi, M.M., Crisco, J.J., Vasavada, A., Oda, T., Cholewicki, J., Nibu, K., Shin, E., 2001. Mechanical properties of the human cervical spine as shown by three-dimensional load-displacement curves. Spine 26, 2692–2700.

Prasad, P., King, A.I., 1974. An experimentally validated dynamic model of the spine. J. Appl. Mech. 41, 546–550.

Siegmund, G.P., Blouin, J.-S., Brault, J.R., Hedenstierna, S., Inglis, J.T., 2007. Electromyography of superficial and deep neck muscles during isometric, voluntary, and reflex contractions. J. Biomech. Eng. 129, 66–77.

Snijders, C.J., Hoek van Dijke, G.A., Roosch, E.R., 1991. A biomechanical model for the analysis of the cervical spine in static postures. J. Biomech. 24, 783–792.

Suderman, B.L., Vasavada, A.N., 2017. Neck muscle moment arms obtained in-vivo from MRI: effect of curved and straight modeled paths. Ann. Biomed. Eng. https://doi.org/10.1007/s10439-017-1830-8.

Suderman, B.L., Krishnamoorthy, B., Vasavada, A.N., 2012. Neck muscle paths and moment arms are significantly affected by wrapping surface parameters. Comput. Methods Biomech. Biomed. Eng. 15, 735–744.

van der Horst, M.J., Thunnissen, J.G.M., Happee, R., van Haaster, R.M.H.P., Wismans, J.S.H.M., 1997. The Influence of Muscle Activity on Head-Neck Response During Impact (SAE Technical Paper No. 973346). SAE Technical Paper, Warrendale, PA.

van Lopik, D.W., Acar, M., 2007. Development of a multi-body computational model of human head and neck. Proc. Inst. Mech. Eng. Part K J. Multi-Body Dyn. 221, 175–197.

Vasavada, A.N., Li, S., Delp, S.L., 1998. Influence of muscle morphometry and moment arms on the moment-generating capacity of human neck muscles. Spine 23, 412–422.

Vasavada, A.N., Lasher, R.A., Meyer, T.E., Lin, D.C., 2008. Defining and evaluating wrapping surfaces for MRI-derived spinal muscle paths. J. Biomech. 41, 1450–1457.

Williams, J.L., Belytschko, T.B., 1983. A three-dimensional model of the human cervical spine for impact simulation. J. Biomech. Eng. 105, 321–331.

Woittiez, R.D., Huijing, P.A., Rozendal, R.H., 1983. Influence of muscle architecture on the length-force diagram. Pflugers Arch. 397, 73–74.

Woittiez, R.D., Huijing, P.A., Boom, H.B., Rozendal, R.H., 1984. A three-dimensional muscle model: a quantified relation between form and function of skeletal muscles. J. Morphol. 182, 95–113.

Woittiez, R.D., Baan, G.C., Huijing, P.A., Rozendal, R.H., 1985. Functional characteristics of the calf muscles of the rat. J. Morphol. 184, 375–387.